E2B - E281

PUB-78-106-E
E-0002
E-0281

Studies of $\pi^- p$ Interactions in the Fermilab Hybrid System*

William D. Shephard
Department of Physics
University of Notre Dame, Notre Dame, Indiana 46556, USA

I. Introduction

During the past year, samples of $\pi^- p$ interactions, observed with the Fermilab hybrid system composed of the 30-inch bubble chamber together with downstream wide-gap optical spark chambers, have been used to study a variety of aspects of hadronic interactions. Significant data samples at several energies allow not only detailed studies at a single value of total energy $\sqrt{s}$ but also studies of the energy dependence of various phenomena. The samples of $\pi^- p$ interactions used for the results reported here include approximately 30,000 events at 360 GeV/c, 17,000 events at 200 GeV/c, and 7700 events at 100 GeV/c. Events of all charge multiplicities are available. Events of each multiplicity are weighted to correspond to published semi-inclusive cross sections[1].

Institutions, in addition to the University of Notre Dame, which have contributed to the various data samples and analyses include Duke University, Fermilab, Iowa State University, University of Maryland, Michigan State University, University of Toronto,

and McGill University. The data were obtained in experiments E2B and E281 at Fermilab.

Topics of study for which new results have been obtained during the past year include: the quark-parton structure of hadrons (both protons and pions); energy dependence of two-charged-particle rapidity correlations; three-particle rapidity correlations; diffraction dissociation cross sections as a function of charge multiplicity; ρ^0 production as a function of energy; and Δ^{++} production as a function of energy. In summarizing these results I will spend most of the time and space on the topics which I believe to be of greatest current interest.

II. The Quark-Parton Structure of Hadrons

One of the most exciting recent developments in hadron physics has been the formulation of methods by which hadron production at low p_T may be used to provide information about the quark-parton structure of the incident hadrons. Results are now available[2,3] on several tests of simple models for low-p_T hadron production which indicate the promise of these models. The results so far available represent only the first stage in a continuing development of our knowledge in this area. The development of models is proceeding at a rapid rate, and the larger samples of data with better secondary particle identification from future experiments with the Fermilab

hybrid system and the CERN EHS will allow more sensitive tests of the details of quark-parton structure functions.

Data from deep inelastic lepton-hadron interactions and from large-p_T hadron production experiments yield information on the hard scattering of elementary hadron constituents (partons) and the subsequent production of hadrons by quark-parton fragmentation. The results give information on the valence quark structure functions of the incident hadrons. For example, Field and Feynman[4] have presented parametrizations for the quark structure functions of the proton using information from these sources; also presented are quark structure functions for pions based mainly on theoretical arguments and physical intuition since there are no data on deep inelastic scattering from pions. It is natural to attempt the extension of quark-parton models to describe processes at small momentum transfer and low p_T. Das and Hwa[5], for example, have shown that the quark-parton model can be successfully applied to low-p_T inclusive particle production, but that the dominant process for secondary particle formation does not appear to be quark fragmentation (which yields a cross section which is too small and falls too fast with Feynman x as a result of the convolution of the structure and fragmentation functions). Instead, the majority of low-p_T meson production appears to come from quark-antiquark recombination. In the range

$0.2 \lesssim x \lesssim 0.6$, where adequate data from the hybrid experiments are available, the dominant process seems to be recombination of a relatively fast valence q or $\bar{q}$ with slow $\bar{q}$ or q either from the original quark sea of the incident hadron or from the sea of virtual $q\bar{q}$ pairs excited by gluons. Hard-scattering interactions such as deep inelastic scattering involve a time scale short enough so that information is provided primarily on distributions of valence quarks and to some extend the distributions of quarks in an instantaneous sea available for interaction. Typically about 40-50% of the momentum of the incident hadron is carried by these hadronic constituents. Duke and Taylor[6] have applied the quark recombination model to data on low-p_T meson production in high energy pp interactions at Fermilab[7] to provide information on the effective sea quark distributions in the proton. They have assumed the Field-Feynman[4] proton valence quark distributions and have parametrized the sea-quark distributions with the simple form $A_q(1-x)^{n_q}$, adjusting the constants A_u, A_d, A_s and the exponents n_u, n_d and n_s to fit the data. They find $n_u \approx n_d \approx 8$ and find evidence for a sea contribution larger than the sea measured in lepton experiments so that essentially the entire momentum of the incident proton is carried by the valence quarks plus the enhanced sea. This is consistent with low-p_T meson production occurring over a time scale long enough

that the gluons create virtual $q\bar{q}$ pairs which are gradually converted to final-state mesons by the recombination process.

We have attempted to extend[2] the quark recombination model of Das and Hwa[5] as developed by Duke and Taylor[6] to provide information on quark structure functions in the pion as well as the proton using data on inclusive π^- and π^+ production in $\pi^- p$ interactions at 200 GeV/c where the available statistics are adequate and the momentum resolution is reasonably good over the kinematic region of interest. Charged secondaries having no obvious kinks and not identified as protons with $p_{lab} < 1.4$ GeV/c are assumed to be pions. According to the model[6], the invariant cross section for inclusive meson production at momentum fraction x is approximated by

$$f(x) = \frac{E}{\sigma_T}\frac{d\sigma}{dp} = c\left(\frac{1-x}{x}\right)\int_0^x F_q(y)\,F_{\bar{q}}(x-y)\,dy \qquad (1)$$

where, e.g., $F_q(y) = \sum_{q,\bar{q}} y\,q(y)$ is the quark content of the incident hadron at momentum fraction y. The summation is taken over those constituents which can contribute to production of mesons of the desired type.

We first check whether backward $\pi^\pm$ production ($0.2 \lesssim -x \lesssim 0.6$) in $\pi^- p$ interactions is consistent with the results of Duke and Taylor[6] for quark distributions in the proton. We use the Field-Feynman[4] valence quark distributions and the Duke-Taylor[6] $u(\bar{u})$ and $d(\bar{d})$

sea quark distributions to compute $f(\pi^+)$, $f(\pi^-)$ and the ratio $R \equiv f(\pi^+)/f(\pi^-)$ as a function of x. In Fig. 1 are shown the experimental data and calculated meson distributions. Agreement is satisfactory in the region where the model is expected to be valid and the data are of reasonable precision. Fig. 1a also shows data on R from Johnson et al.[7] for pp interactions at 200 GeV/c. Since the pp and $\pi^- p$ data agree fairly well it is no surprise that the same proton quark distributions can describe both.

We now analyze the $\pi^- p$ forward $\pi^\pm$ production data ($+0.2 \lesssim x \lesssim +0.6$) in terms of the same model to obtain information about quar distributions in the pion. Since valence quark distributions for the pion are not as well known we assume several reasonable forms. I each case we assume distributions for each of the sea quarks (d, $\bar{d}$, $\bar{u}$) in the incident π^- of the form $F_q(y) = A(1-y)^N$. We then vary both A and N to obtain the best description of the π^+/π^- ratio R as a function of x. The choice of A and N is, however, subject the momentum sum-rule constraint. If the total momentum fractio carried by the valence quarks is f_v, then that carried by the sea quarks must be $\leq (1-f_v)$ and (neglecting $s(\bar{s})$ sea quarks) we have the constraint $4\int_0^1 F_{sea}(y)\,dy = 4A/(N+1) \leq (1-f_v)$. We vary over the range $2 \leq N \leq 6$ in steps of $\Delta N = 1$. Each assumed valen distribution is normalized such that $\int_0^1 (F_{valence}(y)/y)\,dy = 1$ and

then $f_v = 2 \int_0^1 F_{valence}(y)\,dy$.

We present in Fig. 2 the results of our comparison of the experimental values of R as a function of x with distributions calculated using four different forms for the pion valence quark structure functions. These include the Field-Feynman form, a form from Dao et al.[8], and two other simple forms. The assumed valence quark distributions are shown in Fig. 3a. Results are summarized in Table I. In each case we find that for a given N in the sea-quark functions the best agreement with data is obtained with the largest possible A consistent with the momentum sum rule constraint.

From Fig. 2 we draw the following conclusions. Over the range $0.2 < x < 0.6$ the data are reasonably described with valence distributions B and C using N = 4 in the sea-quark distributions. Valence distributions A and D do not provide good descriptions of the data. In the region $x \lesssim 0.6$ we cannot clearly choose between B and C. The Field-Feynman distributions are motivated by theoretical arguments and receive some support from experimental data on high-p_T meson production. Hence they are probably to be preferred. High-statistics data on low-p_T meson production at $x > 0.6$ in $\pi^{\pm}p$ interactions should clearly distinguish between B and C.

In Fig. 3b we show experimental data for $f(\pi^+)$ and $f(\pi^-)$ in the forward hemisphere together with calculated curves from Field-

Feynman valence functions and sea-quark functions $F(y) = 0.85(1-y)^4$. The agreement is generally satisfactory.

We draw the following conclusions from our study: (a) Backward $\pi^{\pm}$ production in π^-p interactions is consistent with the same quark structure functions determined by Duke and Taylor[6] for pp interactions. (b) Forward pion production in π^-p interactions is consistent with the valence quark structure functions suggested by Field and Feynman[4] for pions together with sea-quark structure functions varying as $(1-y)^4$. (c) Approximately the entire momentum of the incident π^- appears to be carried by the valence quarks plus the quarks of the enhanced sea. This is consistent with a picture where the long time scale for low-p_T meson production allows virtual quarks from gluons to interact. (d) Although each valence quark in both pion and proton seems to carry ~15% of the incident particle momentum on average, there is a greater probability for pion valence quarks to carry high momentum. (e) Sea quarks in pions tend to carry more momentum than those in protons.

A next logical step in probing the quark-parton structure of hadrons which will take advantage of the hybrid track chamber data is the study of two-particle inclusive reactions. H.I. Miettinen[9] has suggested that we study correlations between identified fragmentation products in the process

$$A + B \rightarrow a + b + \text{anything} \qquad (2)$$

where a and b are low-p_T fragments of A, each carrying a finite fraction (x_a, x_b) of the c.m. longitudinal momentum of A. In effect we trigger on a fast hadron of a particular type at x_a and study cross sections or ratios thereof for various types of hadrons at x_b. Data for proton fragmentation from our 360 GeV/c experiment have been compared[3] with predictions of a very simple first-order recombination model. Single meson production in the fragmentation region involves primarily the recombination of a valence quark from A with a sea antiquark to form the detected meson "a" at Feynman x_a. Hence

$$F_{a/A} \equiv \frac{1}{\sigma}\frac{d\sigma}{dx_a} = \Sigma \int dx_1 dx_2 \, f_{q\bar{q}/A}(x_1, x_2)\phi_a(x_1, x_2) \, \delta(x_1 + x_2 - x_a) \qquad (3)$$

where the sum runs over $q\bar{q}$ permutations with the quantum numbers of a, $f_{q\bar{q}/A}(x_1, x_2)$ is the probability to find q at x_1 and $\bar{q}$ at x_2, and $\phi_a(x_1, x_2)$ is the probability for the $q\bar{q}$ system to form meson a. Multiquark or quark-gluon components are neglected or assumed to be included in an average way as two quasi-quarks. Since sea quarks are concentrated near $x = 0$, $F_{a/A}(x_a)$ will be approximately proportional to $f_{q/A}(x_a)$, the probability of finding q at x_a in A[10]. We assume sea-sea recombination to be negligible in the x_a region

of interest unless the valence-sea recombination is not allowed by the quantum numbers.

The extension of the model to double fragmentation processes is straightforward[11]. For A a baryon and a and b mesons, we have

$$F_{ab/A}(x_a, x_b) \equiv \frac{1}{\sigma}\frac{d^2\sigma}{dx_a dx_b} = \Sigma \int dx_1 dx_2 dx_3 dx_4 \, f_{q\bar{q}\,q\bar{q}/A}(x_1, x_2, x_3, x_4) \, \phi_a(x_1, x_2)\phi_b(x_3, x_4) \, \delta(x_1 + x_2 - x_a)\, \delta(x_3 + x_4 - x_b) \qquad (4)$$

Again assuming $x \approx 0$ for sea quarks we set $x_2 = x_4 = 0$ yielding

$$F_{ab/A}(x_a, x_b) \sim f_{qq/A}(x_a, x_b) \qquad (5a)$$

A similar formula results if A, a, and b are all mesons. If A and a are baryons and b is a meson, an equation similar to Eq. (5a) again applies, but a second mechanism is also possible in which two valence quarks from A combine with a sea quark to form a. Then

$$F'_{ab/A}(x_a, x_b) \sim \int dx_1 dx_2 \, f_{qqq/A}(x_1, x_2, x_b)\, \delta(x_1 + x_2 - x_a) \qquad (5b)$$

The Kuti-Weisskopf model[12] can be used to derive a scaling relation of the form

$$f_{qq/A}(x_a, x_b) = g(x_a)\, h(\tilde{x}_b) \qquad (6)$$

using the new scaling variable $\tilde{x}_b = \frac{x_b}{1 - x_a}$, the ratio of x_b to its maximum value. However, since the u and d distributions in the proton are known to be different, the Kuti-Weisskopf model must be

modified and Eq. (6) can be only an approximation.

Consider now the predictions of our simple model for two-particle proton (u u d) fragmentation when particle "a" is a K^o ($\approx d\bar{s}$), π^+ ($\approx u\bar{d}$) or π^- ($d\bar{u}$) and "b" is a π^+. Since, in the proton fragmentation region, the trigger hadrons are produced from valence u or d quarks, the probability of producing a π^+ at x_b in conjunction with a K^o, π^+ or π^- at x_a is $f_{qu/p}(x_a, x_b)$ in all cases. The normalizations, however, depend on the relative abundances of $\bar{s}$, $\bar{d}$ and $\bar{u}$ sea quarks. Since in all cases the π^+ at x_b contains a valence u quark, we predict the following relations for the average numbers of π^+ at $\tilde{x}_b$ per trigger particle at x_a:

$$\bar{n}_{\pi^-}(\pi^+) \approx n_{K^o}(\pi^+) \approx 2\bar{n}_{\pi^+}(\pi^+) \tag{7a}$$

assuming the average number (m) of each type of sea quark ($\bar{u}$, $\bar{d}$, u, d) available for recombination is large. For smaller m, simple combinatorics yield

$$\bar{n}_{\pi^-}(\pi^+) \approx \left(\frac{2m}{2m-1}\right) \bar{n}_{K^o}(\pi^+) \approx \left(\frac{m}{m-1}\right) 2\bar{n}_{\pi^+}(\pi^+) \tag{7b}$$

where we have ignored the (small) probability of recombination of a valence quark with a sea $\bar{s}$ and any dispersion in sea-quark multiplicities. In fact, $m \approx 2 - 3$ is expected on the basis of average pion multiplicity in the central region or by considering the fractional contribution of each species to the proton's c.m. momentum.

In the 360 GeV/c π^-p data sample used to test the model, secondary protons with $p_{lab} < 1.4$ GeV/c (corresponding to $x_p \lesssim -0.3$) are identified by ionization and $K^o_s \to \pi^+\pi^-$ decays have been identified. In terms of the model we assume that most K^o_s in the proton fragmentation region are K^o rather than $\bar{K}^o$.

In Fig. 4 we show $\bar{n}_{\pi^-}$, $\bar{n}_{K^o}$ and $2\bar{n}_{\pi^+}$ as a function of $\tilde{x}_{\pi^+}$ for various ranges of trigger x_a. We see that each of these quantities is approximately independent of x_a and that the prediction of $\tilde{x}_b$ scaling holds remarkably well. The shape of these distributions seems independent of the nature of the trigger particle, thus providing additional support for the no-resonance approximation[11], since resonance spectra in $\pi^+\pi^-$ and π^+K^o systems are quite different from that in exotic $\pi^+\pi^+$ systems. The data agree with the predictions of Eq. (7b) that $\bar{n}_{\pi^-} > \bar{n}_{K^o} > 2\bar{n}_{\pi^+}$. With present statistics we cannot quote precise values for the ratios; however, for $|x_a| > 0.2$ the average ratios are consistent with $\bar{n}_{\pi^-}/\bar{n}_{K^o} \sim 1.3$ and $\bar{n}_{\pi^-}/2\bar{n}_{\pi^+} \sim 1.7$ yielding $m \sim 2.2$ and $m \sim 2.4$ consistent with each other and with our expectations.

To test the relative importance of mechanisms (5a) and (5b) we look at data for $\pi^-p \to \pi^-(x_a) + p(x_b)$ + anything in the proton fragmentation region. In Table II we give values for $d\sigma/dx_a dx_b$ in this reaction together with corresponding data for $\pi^-p \to \pi^-(x_a)$ +

$\pi^+(x_b)$ + anything. In the former case we note that the data extend out to the kinematic limit $|x_a| + |x_b| \approx 1$ and that the probability of finding a proton and a trigger π^- is about 18% independent of $x_a(\pi^-)$ for $0.5 > |x_a| > 0.1$. (The value for a proton and a trigger π^+ is about 12%.) For comparison, about 34% of untriggered inelastic events include an identified secondary proton. In the latter case most of the data occur at $|x_a| + |x_b| < 2/3$. The data of Table II are also consistent with scaling in $(x_a + x_b)$ for $|x_a|, |x_b| > 0.1$ as expected from the simple Kuti-Weisskopf model.

The interpretation seems straightforward: dipions are produced from two valence quarks according to Eq. (5a), so $|x_a| + |x_b| < 2/3$ predominates. For $\pi^-(x_a)p(x_b)$ it appears that Eq. (5b) describes the data. The π^- is usually created from a valence d and a sea $\bar{u}$ while the proton is formed by recombination of the remaining two valence u quarks and a sea d quark. We note, however, that the relatively low percentage of events with both a fast p and a fast $\pi^\pm$ trigger suggests that when one valence quark is removed in the trigger the remaining two valence quarks tend to separate and dissociate into two mesons rather than pick up another quark to form a baryon. (Of course baryon number must be conserved in the overall reaction.) Since one of the original motivations for postulating colored vector gluons was to bind the $q\bar{q}$ but not the qq

system, we have a result consistent with QCD.

In summary, the first tests of a simple quark recombination model with data from two-particle inclusive reactions appear quite encouraging. Data from the next generation of hybrid experiments with improved secondary-particle identification will allow further tests to be made.

III. Rapidity Correlations in π^-p Interactions

Previous investigations[13] have clearly established the existence of strong positive short-range correlations in rapidity between charged pions in the central region in high energy inclusive reactions. Short-range semi-inclusive correlations have been shown to exist at fixed charge multiplicities[14, 15], and differences have been shown to exist between the inclusive correlations for like-charge and unlike-charge pairs[15, 16]. We have shown[16] that inclusive like-charge correlations at small rapidity difference Δy depend strongly on the relative angle and magnitude of the transverse momenta consistent with Bose-Einstein symmetrization effects. The correlations for unlike-charge pairs show less dependence on the transverse momenta. A useful way of analyzing the inclusive data has been in terms of the production of "clusters" which subsequently decay into the observed final-state hadrons[13].

With our current data on π^-p interactions at several energies

(including a sample of 7800 events at 18.5 GeV/c) it has been possible to demonstrate clearly the differences between like-charge and unlike-charge semi-inclusive correlations. We have analyzed the energy and multiplicity dependence of the semi-inclusive correlations in terms of an independent cluster emission model as formulated by Berger[17] and have interpreted the results in terms of the cluster parameters $< k >$, the average charged-particle population of a cluster, and δ, the dispersion parameter or correlation length[18].

Data at each energy and multiplicity have been treated in a consistent manner. Events were binned in a $\Delta y = y_1 - y_2$, $y_+ = y_1 + y_2$ coordinate system since the correlations are known to depend on rapidity difference Δy. For each charge multiplicity $n (4 \leq n \leq 20)$ the single-particle densities $\rho_1^n(y) = \sigma_n^{-1} d\sigma/dy$ and two-particle density $\rho_2^n(y_1, y_2) = \sigma_n^{-1} d^2\sigma/dy_1 dy_2$ are determined and used to calculate normalized correlation functions $R_n(y_1, y_2) = R_n(\Delta y, y_+) = [\rho_2^n(y_1, y_2)/(\rho_1(y_1)\rho_1(y_2))] - 1$.

Distributions of the $R_n^{-+}(\Delta y)$ and $R_n^{--}(\Delta y)$ as a function of Δy integrated over a central region $-4.05 \leq y_+ \leq +4.05$ for the 360 GeV/c $\pi^- p$ data are shown in Fig. 5. The inclusive $R(\Delta y)$ are also shown. The $R_n^{++}(\Delta y)$ (not shown) are quite similar to the $R_n^{--}(\Delta y)$. For the (-+) pairs, significant correlation is seen near $\Delta y = 0$ for all n; the magnitude at $\Delta y = 0$ varies linearly as 1/n. For the (--) pairs,

less prominent correlation peaks are seen at all n over a narrower range of Δy; there is no clear n dependence at $\Delta y = 0$ of the peak values and the large-Δy regions exhibit the $1/n_-$ variation expected from the overall normalization in the absence of correlations. If we select on different ranges of ϕ, the angle between the transverse momentum vectors of the particles (see Ref. 16) we find distinct differences for the $R_n^{--}(\Delta y)$ as shown in Fig. 6. For $\phi \leq 45^\circ$ sharp peaks at $\Delta y = 0$ are seen for all n; for $\phi > 45^\circ$ there is little evidence of significant correlation. For (-+) pairs, correlations (not shown) are comparable for both ϕ ranges and appear similar to those for the complete sample.

In terms of Berger's cluster model[17] with a narrow multiplicity distribution one expects

$$R_n^{-+}(0, 0) = \frac{\ln s}{n} \left[\frac{< k >^{-+}}{2\delta\sqrt{\pi}} - \frac{< k >^{-+}}{\ln s} \right]. \tag{8}$$

We have simultaneously fitted Eq. (8) to the data for $R_8^{-+}(0, 0)$ (n = 8 was chosen to provide adequate statistics while avoiding possible probelms with diffractive effects) as a function of $\ln s$ and data for $R_n^{-+}(0, 0)$ at 360 GeV/c (where we have the widest range of n) with $8 \leq n \leq 20$ as a function of 1/n, to determine the cluster parameters. The fit yields $< k >^{-+} = 1.60 \pm 0.12$ and $\delta = 0.99 \pm 0.03$. From Fig. 7 it can be seen that the model provides an excellent description of

the data with these reasonable values of cluster parameters. In contrast the $R_n^{--}(0, 0)$ show no clear variation with $1/n$ and the $R_8^{--}(0, 0)$ are approximately independent of s. Fits of these data with the appropriate cluster model equation analogous to Eq. (8) yield a value for $< k >$ consistent with only one negative charged particle per cluster and do not provide a well-determined value[19] of δ.

These results are all consistent with a picture in which clusters of relatively low charge multiplicity are responsible for the observed (-+) correlations while the (--) correlations are quite different in nature. We note that if (-+) and (--) correlations are indeed produced via different mechanisms, the interpretation of previous results on cluster properties[20] determined in experiments where secondary particle charge was not distinguished are open to question. It should also be pointed out that the numbers quoted here are the results of fits to predictions of a specific simple cluster model and should be interpreted with this fact in mind.

Other features of the distributions in rapidity observed for high energy $\pi^- p$ interactions are of interest. For example, at 360 GeV/c values of $\sigma_n^{-1} d\sigma_n/dy$ in the central region vary approximately as $n^{1.7}$ rather than varying linearly with n as expected in terms of naive independent-cluster-emission models. There is evidence for more events with large numbers of final-state particles near $y^* = 0$

in the c.m. than might be expected from simple considerations. We are investigating the characteristics of these events in an attempt to learn more about how they are produced.

Another subject of interest is whether there occur significant three-particle rapidity correlations apart from those produced by the convolutions of the known two-particle correlations. Previous studies[20-22] have yielded no clear evidence of additional three-particle correlations in pp interactions within the limits of available statistics. In 200 GeV/c $\pi^- p$ interactions we observe[23] a small positive three-particle correlation for the (-+-) state (above that estimated from the observed two-particle correlations) when the rapidity differences between all three particles are small. No such effect is seen for (---) systems. The observed three-particle correlations are weak compared to the two-particle correlations. This is in agreement with a picture where the correlations are due to clusters of relatively low charge multiplicity[24]; the absence of (---) clustering, which would require a large charge exchange in the rapidity chain, is not unexpected.

IV. Diffraction Dissociation

For non-diffractive $\pi^- p$ interactions at high energy we find that the dependence of the cross section on charge multiplicity in each c.m. hemisphere exhibits approximate KNO scaling. We classify all in-

elastic events by their forward, backward (n_F, n_B) multiplicities. All the data in the (even, even) subset can be described by the same empirical KNO-type function. Assuming that the non-diffractive part of the (odd, odd) subset can be represented by this same function we can extract values of the non-diffractive and hence, of the diffractive cross sections for each (n_F, n_B)[19]. Details of the procedure and results at 200 GeV/c have been submitted for publication[25]. This technique for extracting diffractive cross sections presents a useful alternative to more conventional methods based on Feynman x, missing-mass, or momentum-transfer distributions.

Preliminary results at 100, 200 and 360 GeV/c are summarized in Table III. The estimated total cross sections for diffraction dissociation in $\pi^- p$ interactions are comparable to the corresponding elastic cross sections. The results are consistent within errors with either a constant diffraction cross section or one rising by perhaps 10% over the available energy range. This method yields a larger cross section and larger mean charge multiplicity for pion dissociation than for proton dissociation. On the basis of factorization arguments, we estimate the cross section for double diffractive dissociation to be ~ 0.5 mb. We note that our technique may lead to an underestimate of diffractive dissociation at high multiplicity since some particles from the decay of high-mass systems may cross over to the

opposite hemisphere, thus contributing to the (even, even) subset. However, other methods have comparable difficulties in estimating diffraction at high mass and high multiplicities.

V. Inclusive and Semi-Inclusive Resonance Production

Results have been obtained[26, 27] on inclusive and semi-inclusive ρ^o and Δ^{++} production as a function of energy in $\pi^- p$ interactions. Only a brief summary of the results will be presented here.

Inclusive and semi-inclusive ρ^o production cross sections are given in Table IV. We find that all our data for $\langle \rho^o \rangle_n = \sigma_n(\rho^o)/\sigma_n$ can be represented by the expression $\langle \rho^o \rangle_n = (0.067 \pm 0.003)n - (0.153 \pm 0.033)$ with $\chi^2/DF = 1.17$. This same expression adequately describes other published data on semi-inclusive ρ^o production in $\pi^- p$ interactions. It may be combined with experimental data on the σ_n or with parametrizations for σ_n such as the KNO scaling formula to provide predictions of $\sigma_n(\rho^o)$ at other energies. Both the inclusive $\sigma(\rho^o)$ and $\langle \rho^o \rangle$ are consistent with a rise of the form $A + B \ln s$ over our energy range. Values of $\langle \rho^o \rangle / \langle \pi_c \rangle$ (where $\langle \pi_c \rangle$ is an estimate of the number of "produced" $\pi^\pm$ pairs) appear to approach the same constant value of ~ 0.12 at large s in both $\pi^\pm p$ and pp interactions.

The y^* and p_T^2 dependence of ρ^o production seem qualitatively similar to that of produced π^+ in $\pi^- p$ interactions. At intermediate p_T^2 $(1.0 < p_T^2 < 2.0\ (\mathrm{GeV}/c)^2)$ the ratio of ρ^o/π^+ is ~ 0.5. The observed ρ^o production appears predominantly central in nature.

In Table V are presented cross sections for semi-inclusive and inclusive Δ^{++} production for $|t_{p\Delta}| < 1\ \mathrm{GeV}^2$ (a region where the limitation of proton identification to $p_{lab} < 1.4$ GeV/c introduces no biases) obtained from fits to π^+p mass distributions and from counting π^+p combinations in the mass range $1.12 < M(\pi^+p) < 1.32$ GeV. The cross sections show no clear energy dependence. Invariant cross sections as a function of x and p_T^2 also show little dependence on incident energy. We find many features of Δ^{++} production to be consistent with a one-pion-exchange mechanism. We find that at 360 GeV/c no more than about 1/3 of the Δ^{++} appear to come from decay of low-mass $\Delta^{++}\pi^-$ systems and that $\lesssim 10\%$ of the Δ^{++} seem associated with diffractively-produced N^* states. Most of this diffractive contribution to final-state Δ^{++} production is in the 4-prong events.

VI. Acknowledgments

I wish to thank my collaborators in the Fermilab E2B and E281 experiments for permission to present our results before final publication. Work at the various institutions was supported in part by the National Science Foundation, the U.S. Department of Energy, and the National Research Council of Canada.

References

* Invited talk at the IX International Symposium on High Energy Multiparticle Dynamics, Tabor, Czechoslovakia, July 2-7, 1978.

1. A.Firestone et al., Phys. Rev. D14, 2902 (1976); D. Ljung, et al., Phys. Rev. D15, 3163 (1977); E.L. Berger et al., Nucl. Phys. B77, 365 (1974).
2. N.N. Biswas et al., "Valence and Sea Quark Distributions in the Pion," to be submitted for publication (1978).
3. E. Lehman et al., "Tests of the Quark-Parton Model in Soft Hadronic Processes," submitted to Phys. Rev. D (1978).
4. R.D. Field and R.P. Feynman, Phys. Rev. D15, 2590 (1977).
5. See K.P. Das and R.C. Hwa, Phys. Lett. 68B, 459 (1977) and the references constained therein.
6. D.W. Duke and F.E. Taylor, Phys. Rev. D17, 1788 (1978).
7. J.R. Johnson et al., Phys. Rev. D17, 1292 (1978).
8. F.T. Dao et al., Phys. Rev. Lett. 39, 1388 (1977).
9. H.I. Miettinen, private communication (1978).
10. By (longitudinal) Lorentz invariance ϕ cannot depend on $x_a = x_1 + x_2$. Since we expect $\phi_a(x_1, x_2)$ to depend on x_1/x_a and x_2/x_a, with $x_2 \approx 0$ the arguments of ϕ become fixed near

0 and 1. Hence $\phi_a(x_1, x_2)$ is treated as a constant.

11. We ignore possible effects of resonance production and decay. A similar no-resonance approximation is made in Refs. 2, 5 and 6 which successfully describe single-particle fragmentation.

12. J. Kuti and V. F. Weisskopf, Phys. Rev. D4, 3418 (1971).

13. See. e.g. J. Whitmore, Physics Reports 27C (1976) and L. Foa, Physics Reports 22C (1975) for summaries.

14. N.N. Biswas et al., Phys. Rev. Lett. 35, 1059 (1975).

15. B.Y. Oh et al., Phys. Lett. 56B, 400 (1975).

16. N.N. Biswas et al., Phys. Rev. Lett. 37, 175 (1976).

17. E.L. Berger, Nucl. Phys. B85, 61 (1975) and private communication.

18. V.P. Kenney et al., "Energy and Multiplicity Dependence of Two-Particle Correlations in 18.5, 100, 200, and 360 GeV/c π^-p Inclusive Reactions," paper submitted to the XIX International Conference on High Energy Physics, Tokyo, Japan (1978).

19. R.L. Bolduc, University of Notre Dame Ph.D. Dissertation (1978) (unpublished).

20. S.R. Amendolia et al., Nuovo Cimento 31A, 17 (1976); K. Eggert et al., Nucl. Phys. B86, 201 (1975)

21. T. Kafka et al., Phys. Rev. D16, 1261 (1977).

22. M. Pratap et al., Nucl. Phys. B116, 1 (1976).

23. N.N. Biswas et al., "Observation of Three-Particle Correlations in Inclusive π^-p Reactions at 200 GeV/c," to be submitted to Nucl. Phys. (1978).

24. Results from a study of the same data using a generalized multiparticle rapidity gap method also suggest that clusters consist predominantly of only two charged particles. See J.W. Lämsä et al., Nucl. Phys. B135, 258 (1978).

25. J.W. Lämsä et al., "The Inelastic Diffractive Dissociation Cross Section in π^-p Interactions at 200 GeV/c," submitted to Phys. Rev. D (1978).

26. P.D. Higgins et al., "ρ^0 Production in π^-p Interactions at 100, 200, and 360 GeV/c," submitted to Phys. Rev. D (1978).

27. P.D. Higgins et al., "Study of Δ^{++} Production in π^-p Interactions at 100, 200, and 360 GeV/c," submitted to Phys. Rev. D (1978).

Table I

Pion Valence Quark Distributions
and Constraints for Sea-Quark Distributions

Valence Dist. F(y)	Total Valence Momentum f_v	Sea-Quark Distribution	Total Sea Momentum f_{sea}	Maximum f_{sea}	A_{max} for N = 4
A (3/4) $\sqrt{y}$ (1 - y)	2/5	$A(1-y)^N$	4A/(N + 1)	3/5	0.75
B (15/16) $\sqrt{y}$ $(1-y)^2$	2/7	$A(1-y)^N$	4A/(N + 1)	5/7	0.89
C Field-Feynman [a)]	0.32	$A(1-y)^N$	4A/(N + 1)	0.68	0.85
D Dao et al. [b)]	0.42	$A(1-y)^N$	4A/(N + 1)	0.58	0.725

a) See Reference 4.

b) See Reference 8.

Table II

$d^2\sigma/dx_a dx_b$ for $\pi^- p_b$, $\pi_a^- \pi_b^+$ at 360 GeV/c

$\lvert x_b(p)\rvert$ \ $\lvert x_a(\pi^-)\rvert$	0.7–0.6	0.6–0.5	0.5–0.4	0.4–0.3	0.3–0.2	0.2–0.1	0.1–0.0
1.0–0.9					0.3	0.9	35
0.9–0.8					--	5.8	63
0.8–0.7				1.4	16	99	
0.7–0.6			0.9	5.1	21	112	
0.6–0.5		0.3	2.2	8.4	23	147	
0.5–0.4	0.3	2.9	4.0	6.2	21	113	
0.4–0.3	--	0.3	1.2	2.1	3.3	9.2	42

$\lvert x_b(\pi^+)\rvert$ \ $\lvert x_a(\pi^-)\rvert$	0.8–0.7	0.7–0.6	0.6–0.5	0.5–0.4	0.4–0.3	0.3–0.2	0.2–0.1	0.1–0.0
0.7–0.6								2.1
0.6–0.5							0.8	3.8
0.5–0.4						0.3	3.5	24
0.4–0.3					3.9	--	7.4	56
0.3–0.2				1.9	9.5	20	139	
0.2–0.1			0.3	5.1	26	79	453	
0.1–0.0		0.7	3.3	26	70	255	1417	
0.0	1.3	7.0	26	70	255	1417		
	4.9	7.6	53	96	288	1771	8106	

The solid lines are drawn for $|x_a| + |x_b| \simeq 1$ and $\simeq 2/3$. The statistical errors may be estimated from the normalization of 3 μb/event.

Table III

Diffractive Cross Sections (in mb) as a Function of Forward-Backward Multiplicities in 100, 200, and 360 GeV/c $\pi^- p$ Interactions

$\sigma_{diff}(n_F, n_B)$ [a]	100	200	360
$\sigma^{\pi}(1,1)$	0.50 ± .07	0.71 ± .05	0.70 ± .04
$\sigma^{\pi}(3,1)$	1.17 ± .16	1.11 ± .09	1.00 ± .07
$\sigma^{\pi}(5,1)$	0.35 ± .13	0.34 ± .07	0.39 ± .05
$\sigma^{\pi}(7,1)$	0.14 ± .07	0.13 ± .06	0.14 ± .03
$\sigma^{\pi}(9,1)$	0.05 ± .04	0.03 ± .03	0.05 ± .02
σ^{π}_{diff}(total)	2.21 ± .23	2.32 ± .14	2.28 ± .10
$\sigma^{P}(1,1)$	0.69 ± .17	0.61 ± .08	0.54 ± .08
$\sigma^{P}(1,3)$	0.46 ± .12	0.50 ± .07	0.72 ± .07
$\sigma^{P}(1,5)$	0.07 ± .07	0.10 ± .04	0.21 ± .05
$\sigma^{P}(1,7)$	0.00 ± .04	0.02 ± .03	0.06 ± .03
$\sigma^{P}(1,9)$	0.00 ± .03	0.00 ± .02	0.02 ± .02
σ^{P}_{diff}(total)	1.22 ± .23	1.28 ± .12	1.55 ± .09
σ_{diff}(total)	3.43 ± 0.31	3.60 ± 0.18	3.83 ± .15

[a] includes double diffraction dissociation where an initial particle dissociates into only one charged particle.

Table IV

Semi-Inclusive and Inclusive ρ^0 Production Cross Sections[a] (in mb)

	p_{lab} (GeV/c)		
n	100	200	360
4	0.77 ± 0.16	0.47 ± 0.11	0.25 ± 0.05
6	1.54 ± 0.25	0.88 ± 0.18	0.74 ± 0.13
8	2.11 ± 0.46	2.12 ± 0.27	1.14 ± 0.23
10	1.16 ± 0.50	1.82 ± 0.25	1.87 ± 0.19
12	1.23 ± 0.45	1.89 ± 0.20	1.57 ± 0.15
14	0.83 ± 0.43	1.12 ± 0.20	1.08 ± 0.15
(≥) 16	0.22 ± 0.20	0.29 ± 0.27	1.03 ± 0.23
(≥) 18		0.18 ± 0.18	0.36 ± 0.12
20			0.24 ± 0.05
(≥) 22			0.0 ± 0.10
Inclusive			
A. (Sum)	7.86 ± 0.99	8.77 ± 0.63	8.28 ± 0.48
B. (Inclusive fit)	7.49 ± 1.79	8.36 ± 0.80	8.49 ± 0.29
C. (Sum of y^*-region fits)	7.60 ± 0.55	8.40 ± 0.72	8.65 ± 0.23
D. (Weighted average of A, B, C)[b]	7.65 ± 0.46	8.54 ± 0.41	8.55 ± 0.17

[a] Errors include some allowance for uncertainties in the fit parametrization.

[b] In computing D, determinations A, B, and C have been treated as independent. The quoted errors on the weighted average do not include any additional contribution for systematic uncertainties.

Table V

Cross Sections (mb) for Δ^{++} Production at $|t_{p\Delta}| < 1\ \mathrm{GeV}^2$ in $\pi^- p$ Interactions at 100, 200, and 360 GeV/c

A. Fits to $M(p\pi^+)$ Distributions

n	P_{lab} 100 GeV/c	200 GeV/c	360 GeV/c
4	0.40 ± 0.05	0.24 ± 0.04	0.31 ± 0.03
6	0.55 ± 0.06	0.35 ± 0.04	0.37 ± 0.04
8	0.30 ± 0.07	0.37 ± 0.05	0.36 ± 0.04
10	0.12 ± 0.05	0.33 ± 0.04	0.24 ± 0.04
12	0.04 ± 0.05	0.12 ± 0.04	0.13 ± 0.03
≥14	---	0.02 ± 0.01	0.08 ± 0.03
Total	1.52 ± 0.15	1.45 ± 0.12	1.56 ± 0.10

B. Cross Section for $1.12 < M(p\pi^+) < 1.32$ GeV

4	0.30 ± 0.02	0.20 ± 0.02	0.23 ± 0.01
6	0.41 ± 0.03	0.27 ± 0.02	0.27 ± 0.01
8	0.31 ± 0.04	0.27 ± 0.02	0.28 ± 0.02
10	0.11 ± 0.02	0.23 ± 0.02	0.20 ± 0.01
12	0.06 ± 0.02	0.09 ± 0.01	0.14 ± 0.01
14	0.00 ± 0.01	0.03 ± 0.01	0.07 ± 0.01
≥16	---	0.02 ± 0.01	0.06 ± 0.02
Sum	1.20 ± 0.06	1.11 ± 0.04	1.25 ± 0.03

Figure Captions

Fig. 1 (a) $f(\pi^+)/f(\pi^-)$ ratio R as a function of x for $x < 0$; (b) Invariant π^+ production cross section $f(\pi^+)$ for $x < 0$; (c) Invariant π^- production cross section $f(\pi^-)$ for $x < 0$ in 200 GeV/c $\pi^- p$ interactions. The curves are calculated with Eq. 1 using Field-Feynman valence-quark and Duke-Taylor sea-quark structure functions for the proton.

Fig. 2 (a) - (d) $f(\pi^+)/f(\pi^-)$ ratio R as a function of x for $x > 0$ in 200 GeV/c $\pi^- p$ interactions. The curves are calculated with Eq. 1 as described in the text using valence-quark distributions A - D of Table I for the pion.

Fig. 3 (a) Pion valence-quark distributions A - D of Table I; (b) Invariant π^+ and π^- production cross sections for $x > 0$ in 200 GeV/c $\pi^- p$ interactions. The curves are calculated with Eq. 1 using Field-Feynman valence quark and $0.85\ (1 - y)^4$ sea-quark structure functions for the pion.

Fig. 4 The average π^+ multiplicity per trigger particle as a function of $\tilde{x}_b = \tilde{x}_{\pi^+}$ for various values of x_a of the π^-, K^o and π^+ trigger in 360 GeV/c $\pi^- p$ interactions. Note that the π^+ trigger data have been multiplied by 2

(see text). A common line with the same absolute normalization has been drawn for purposes of comparison.

Fig. 5 Semi-inclusive correlations $R_n(\Delta y, y_+)$ as a function of Δy integrated over a central region $-4.05 \leq y_+ \leq +4.05$ for 360 GeV/c $\pi^- p$ interactions. (a) Correlations for (-+) pairs; (b) Correlations for (--) pairs.

Fig. 6 Semi-inclusive correlations (--) $R_n^{--}(\Delta y, y_+)$ as a function of Δy for two ranges of ϕ, the angle between the transverse momenta of the particles: (a) $0 \leq \phi \leq 45^o$; (b) $45^o < \phi < 180^o$.

Fig. 7 Energy and multiplicity dependence of the correlation functions $R_n^{-+}(0, 0)$ for unlike-charge pairs: (a) $R_n^{-+}(0, 0)$ as a function of 1/n for 360 GeV/c $\pi^- p$ interactions; (b) $R_n^{-+}(0, 0)$ as a function of s for n = 8 events. The lines represent fits with an independent cluster emission model described in the text.

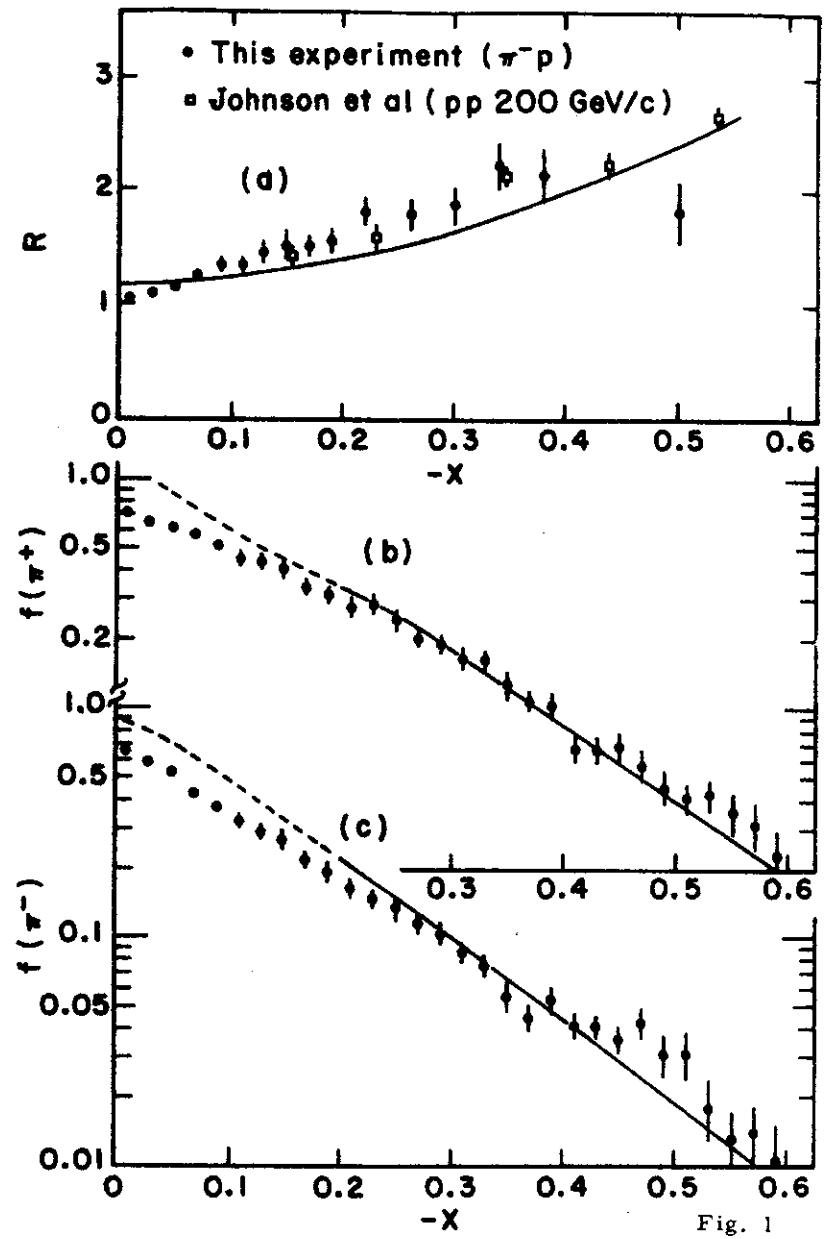

Fig. 1

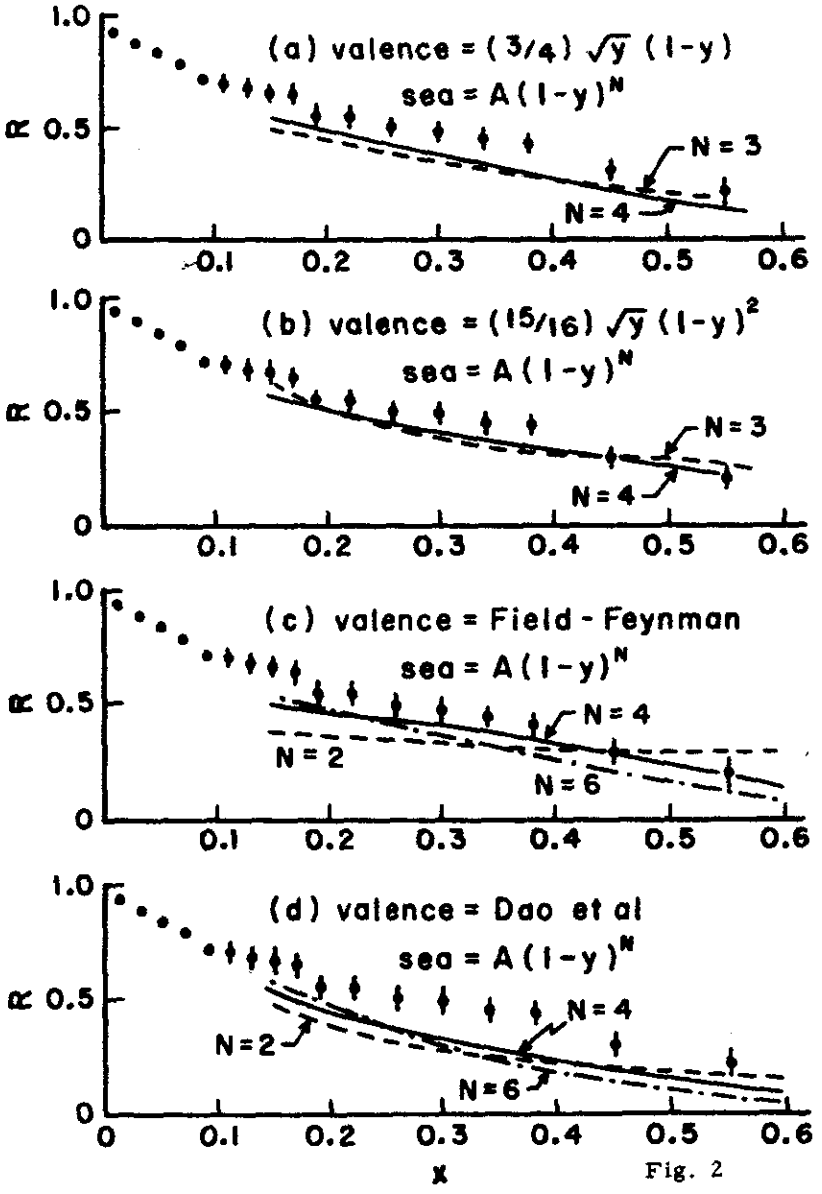
(a) valence = (3/4) √y (1-y)
sea = A(1-y)^N
N = 3
N = 4
(b) valence = (15/16) √y (1-y)^2
sea = A(1-y)^N
N = 3
N = 4
(c) valence = Field - Feynman
sea = A(1-y)^N
N = 4
N = 2
N = 6
(d) valence = Dao et al
sea = A(1-y)^N
N = 4
N = 2
N = 6
R
x

Fig. 2

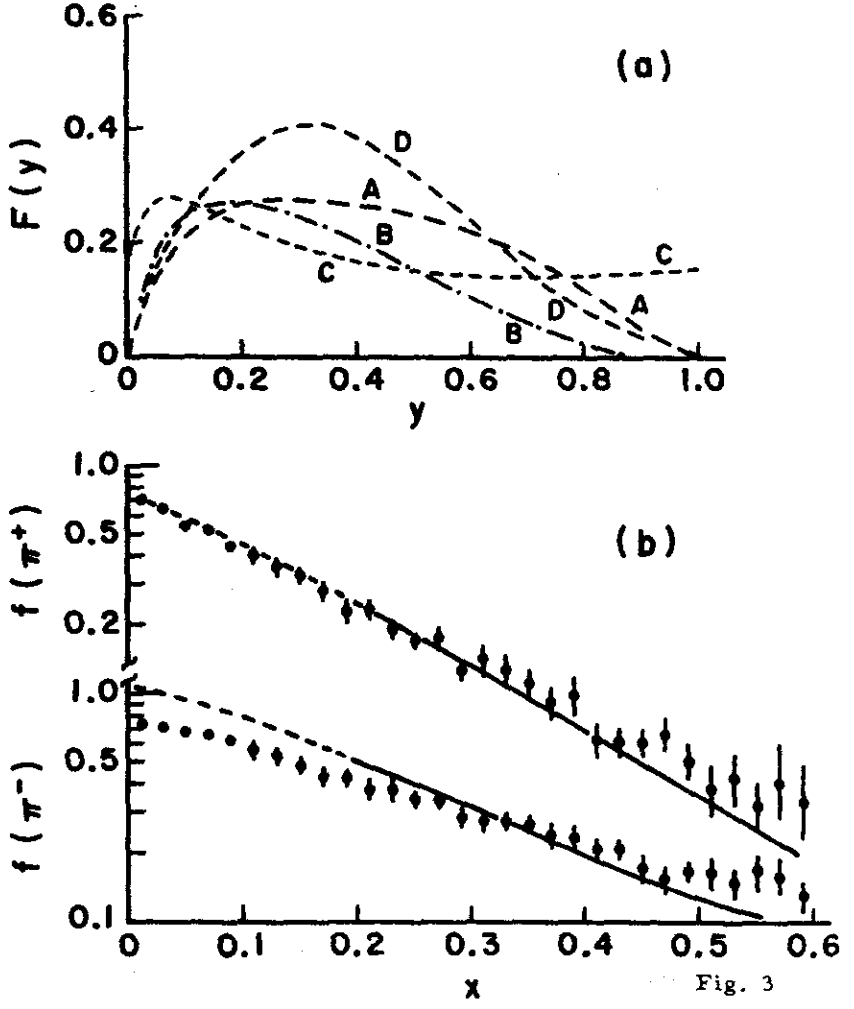
(a)
F(y)
y
A
B
C
D
(b)
f(π+)
f(π−)
x

Fig. 3

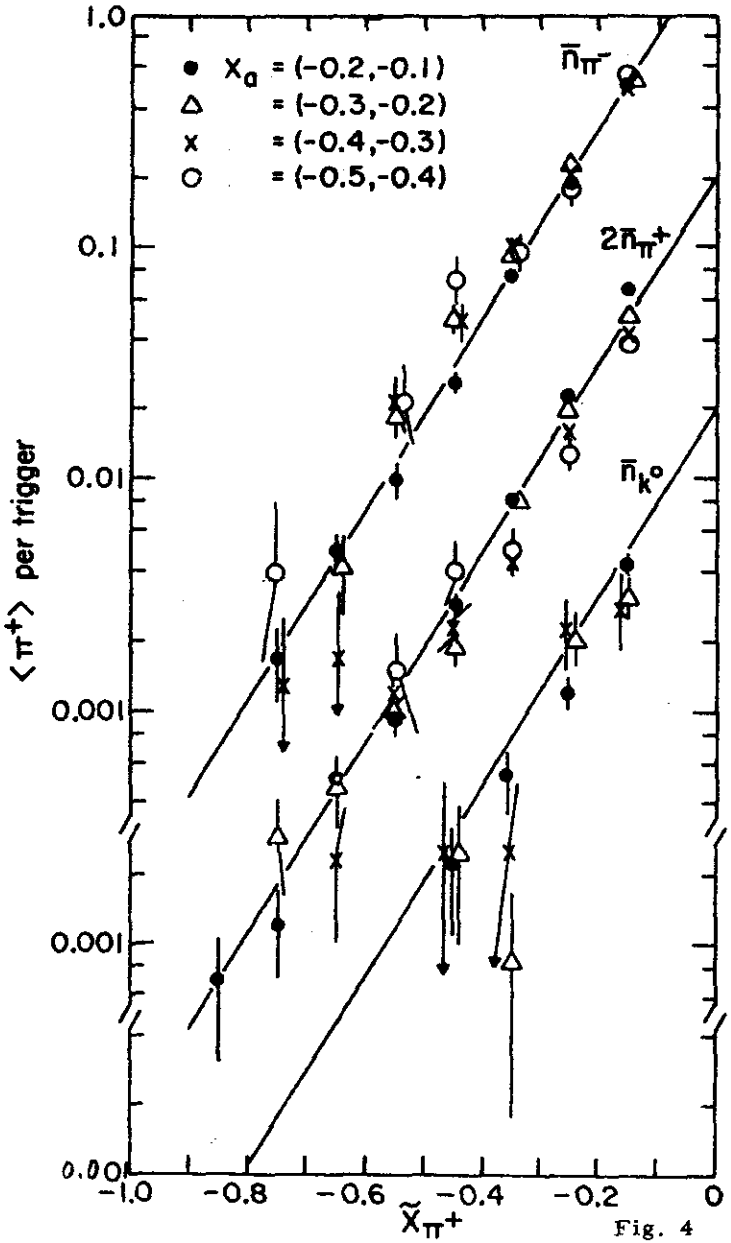
1.0
0.1
0.01
0.001
0.001
0.00
X_a = (-0.2,-0.1)
= (-0.3,-0.2)
= (-0.4,-0.3)
= (-0.5,-0.4)
$\bar{n}_{\pi^-}$
$2\bar{n}_{\pi^+}$
$\bar{n}_{K^0}$
$\langle \pi^+ \rangle$ per trigger
-1.0
-0.8
-0.6
-0.4
-0.2
0
$\tilde{X}_{\pi^+}$

Fig. 4

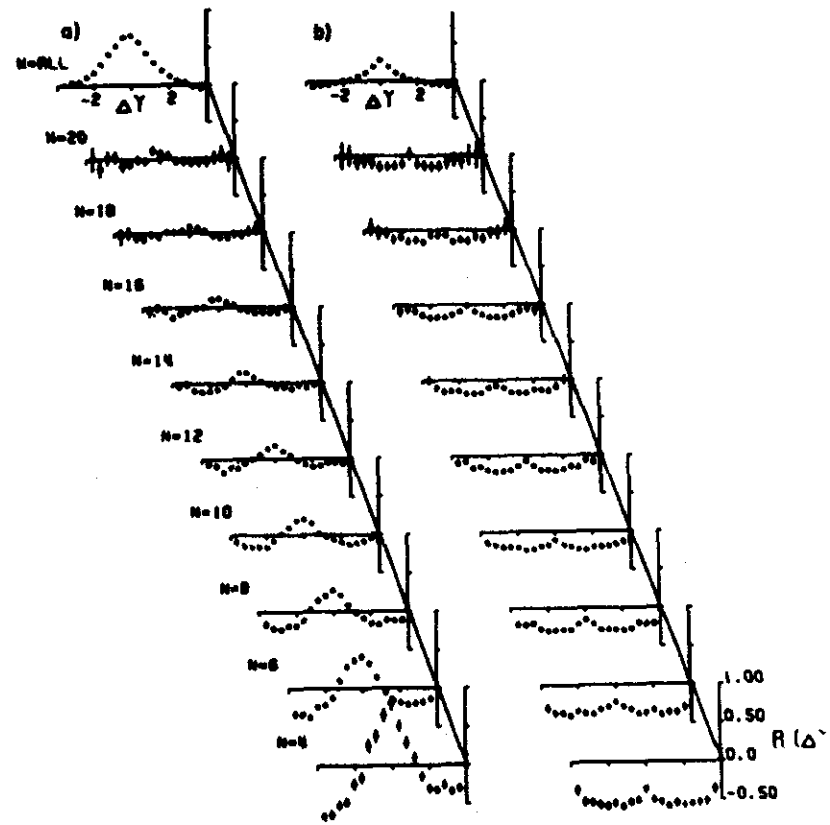
a)
b)
N=ALL
N=20
N=18
N=16
N=14
N=12
N=10
N=8
N=6
N=4
-2
ΔY
2
1.00
0.50
0.0
-0.50
R (Δ

Fig. 5

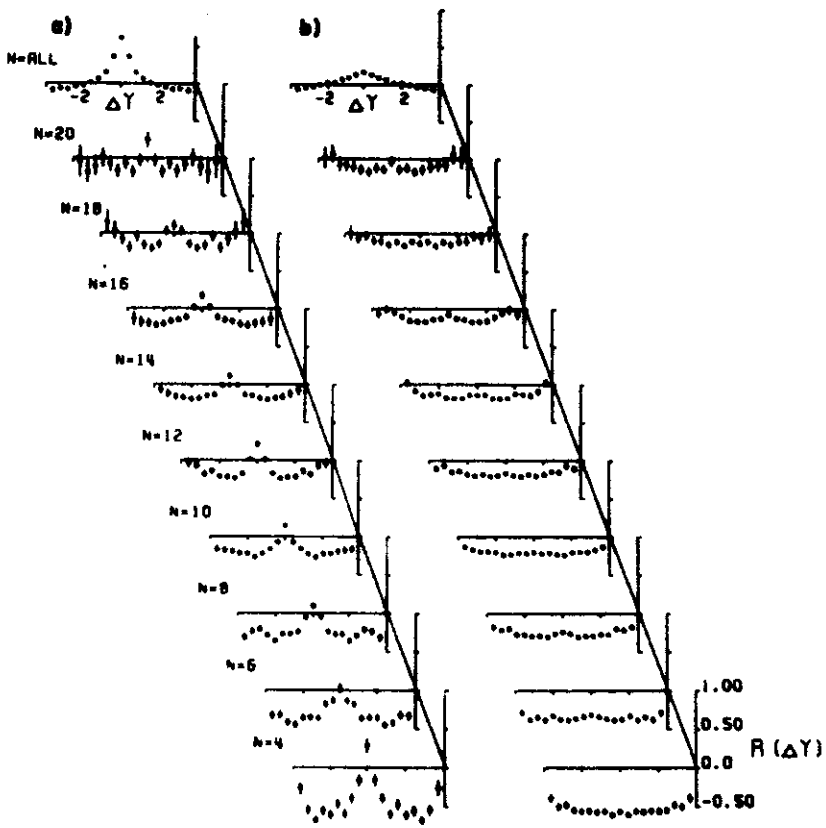
a)
b)
N=ALL
N=20
N=18
N=16
N=14
N=12
N=10
N=8
N=6
N=4
-2 ΔY 2
-2 ΔY 2
1.00
0.50
0.0
-0.50
R (ΔY)

Fig. 6

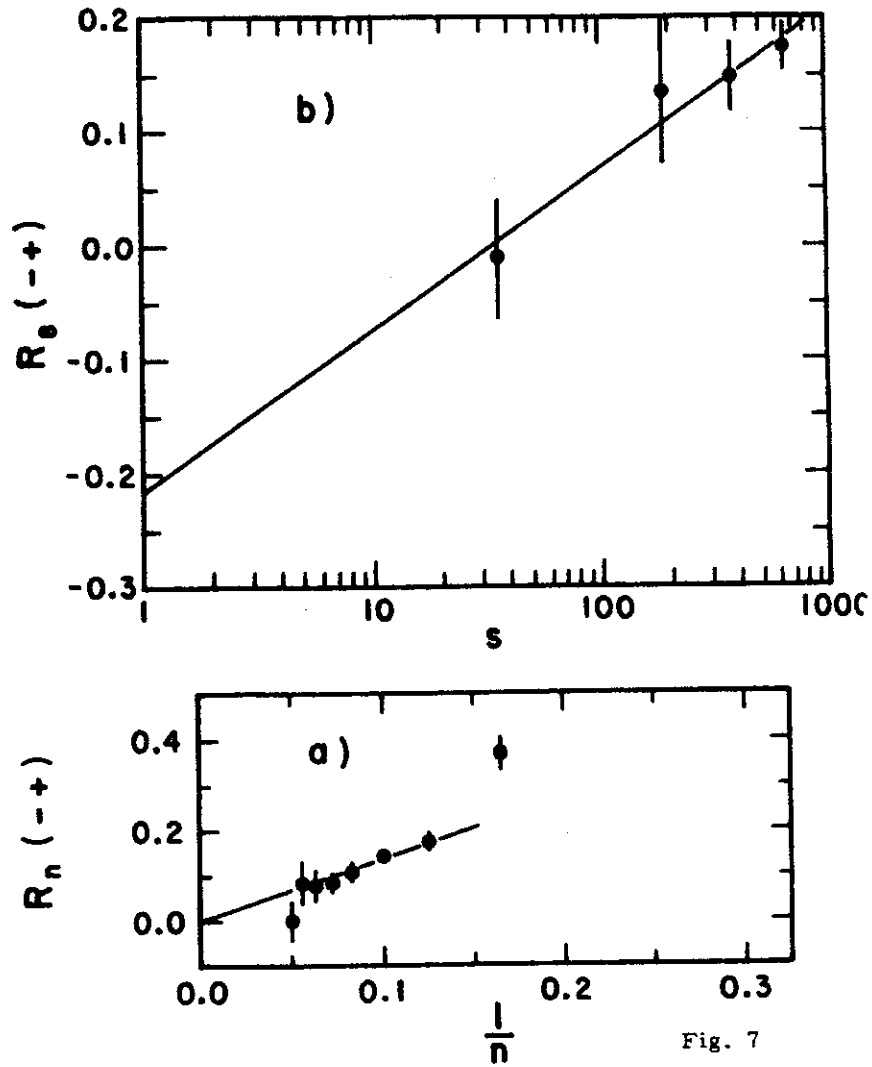
b)
0.2
0.1
0.0
-0.1
-0.2
-0.3
R_s (-+)
1
10
100
1000
s
a)
0.4
0.2
0.0
R_n (-+)
0.0
0.1
0.2
0.3
$\frac{1}{n}$

Fig. 7